A novel interaction between Gβγ and RNA polymerase II regulates cardiac fibrosis

Shahriar M. Khan[†], Ryan D. Martin[†], Celia Bouazza, Jace Jones-Tabah, Andy Zhang, Sarah MacKinnon, Phan Trieu, Sarah Gora, Paul B.S. Clarke, Jason C. Tanny[*], Terence E. Hébert[*]

[1]Department of Pharmacology and Therapeutics, McGill University, Montréal, Québec, H3G 1Y6, Canada

† These authors contributed equally to the manuscript.

*To whom correspondence should be addressed.

Dr. Terence E. Hébert, PhD,

Department of Pharmacology and Therapeutics,

McGill University,

3655 Promenade Sir-William-Osler, Room 1303

Montréal, Québec, H3G 1Y6, Canada

Tel: (514) 398-1398

E-mail: terence.hebert@mcgill.ca

OR

Dr. Jason C. Tanny, PhD,

Department of Pharmacology and Therapeutics,

McGill University,

3655 Promenade Sir-William-Osler, Room 1303

Montréal, Québec, H3G 1Y6, Canada

Tel: (514) 398-3608

E-mail: jason.tanny@mcgill.ca

SUMMARY

Gβγ subunits are involved in an array of distinct signalling processes in various compartments of the cell, including the nucleus. To gain further insight into the functions of Gβγ complexes, we investigated the functional role of Gβγ signalling in the regulation of signal-responsive gene expression in primary cardiac fibroblasts. Here, we demonstrate that, following activation of the angiotensin type I receptor, Gβγ dimers interact with RNA polymerase II (RNAPII) to directly regulate transcription of fibrotic genes. This interaction was specific for complexes containing the $G\beta_1$ subtype and preferentially occurred with the elongating form of RNAPII. The Gβγ/RNAPII interaction was detected in multiple cell types in response to diverse signalling pathways, suggesting that it may be a general feature of signal-responsive transcriptional regulation. Taken together, our studies reveal a novel interaction between Gβγ subunits and RNAPII, further shedding light on the diverse roles Gβγ dimers play in cardiac fibrosis and in GPCR signalling.

1. INTRODUCTION

In recent years, the role of cardiac fibroblasts in paracrine interactions with cardiomyocytes in responses to cardiac stresses during the initiation and progression of heart disease has expanded dramatically. Cardiac fibroblasts proliferate in areas of muscle damage in the heart aiding in wound healing, but ultimately differentiate into myofibroblasts which secrete numerous factors that drive pathological cardiac remodeling [1-6]. Activation of TGF-β, endothelin-1 (ET-1) and angiotensin II (Ang II) receptor signalling have been extensively described to be important mediators of pro-fibrotic responses in cardiac fibroblasts. Ang II has been found to be an important driving factor in fibrotic responses [7, 8] in driving the activities of both TGF-β and ET-1 signalling pathways [9]; examples of such Ang II-dependent effects include the upregulation of TGF-β1 [10, 11] and ET-1 expression [12]. Furthermore, Ang II treatment is known to induce gene expression directly via its own signalling pathways, for example the expression of pro-fibrotic genes such as Ctgf [9, 13], or indirectly mediated by TGF-β and ET-1 signalling, driving expression of genes like collagen I [9, 14]. Inhibiting aspects of the fibrotic response may actually reduce adverse cardiac remodelling [15, 16]. Deciphering the mechanisms of how Ang II signalling regulates gene expression in fibrosis is important to understand how such events might be targeted therapeutically.

Heterotrimeric G proteins, specific combinations of Gα, Gβ and Gγ subunits, act as signal transducers that relay extracellular stimuli sensed by G protein-coupled receptors (GPCRs), such as the type II receptor for Ang I (AT1R), to the activation of distinct intracellular signalling pathways (reviewed in [17]). Of these subunits, Gβ and Gγ form obligate dimers. Gβγ subunits

have been shown to modulate a wide variety of canonical GPCR effectors at the cellular surface such as adenylyl cyclases, phospholipases and inwardly rectifying potassium channels [17-19]. However, Gβγ signalling is more complex than originally imagined. Gβγ subunits have been found to affect a variety of non-canonical effectors in distinct intracellular locations and a number of studies have implicated roles for Gβγ signalling in the nucleus (reviewed in [17, 20]).

Crosstalk between cardiomyocytes and cardiac fibroblasts has been implicated in the progression of cardiac hypertrophy and remodeling of the heart in cardiovascular disease [21]. One key driver of cardiac hypertrophy and fibrosis is Ang II. Previous studies have demonstrated a role for Gβγ signalling in cardiac fibrosis [22, 23]. Bulk inhibition of Gβγ signalling using gallein or GRK2-CT were shown to attenuate the fibrotic response and indeed to reduce cardiac remodelling [22, 24, 25]. To understand the potential role of individual Gβγ subunits in the cardiac fibrotic response to Ang II activation of AT1R, we knocked down $G\beta_1$ and $G\beta_2$ as key exemplars of Gβ subunits in these cells and characterized how $G\beta_1$ in particular is a key regulator of the fibrotic response. Unexpectedly, our results revealed a direct role for Gβγ in regulation of transcription that is important for its role in fibrosis.

RESULTS

The role of Gβγ subunits in cardiac fibrosis.

We assessed the role of individual Gβ subunits on Ang II-induced gene expression in rat neonatal cardiac fibroblasts (RNCF) by knockdown of $G\beta_1$ and $G\beta_2$. We first validated the knockdown conditions using siRNA at the mRNA and protein level (Supplemental Figure 1). Using a qPCR-based gene expression profiling array, we assessed expression of 84 genes known to be regulated in the fibrotic response driven by Ang II and other mediators. Levels of eleven of these genes remained below our chosen limit of detection (i.e. Ct > 35) and were excluded from further analysis. In response to Ang II treatment, we observed significant increases (fold change>2.0, $p<0.05$) in the expression of eight genes with trends for upregulation (fold change>2.0) of a further 15 genes (Supplemental Table 1). Thus, we could easily detect a fibrotic response following Ang II treatment where expression levels of 23 genes were increased.

Knockdown of $G\beta_1$ followed by stimulation with Ang II showed trends for increase in expression of 37 genes (Supplemental Table 1). Interestingly, $G\beta_1$ knockdown alone resulted in a significant basal upregulation of 19 genes (Supplemental Table 1). These results suggested that $G\beta_1$ acts as the key regulator of gene expression and its specific absence dysregulates the fibrotic response. In contrast, knockdown of $G\beta_2$ resulted in significant upregulation of four genes and downregulation of three genes (Supplemental Table 1). Overall the response to Ang II stimulation was not much different from control when $G\beta_2$ was knocked down with 23 genes upregulated in response to Ang II compared to 19 with control siRNA (Supplemental Table 1). In general, the effects of $G\beta_2$ knockdown were less striking than $G\beta_1$ suggesting that other Gβ

subunits in the cardiac fibroblast might be able to substitute for some $G\beta_2$ functions and that the effect of $G\beta_1$ is unique. We next explored the mechanistic underpinnings of this phenomenon.

Gβγ interactions with transcriptional regulators.

We have previously shown that Gβγ interacts with cFos to decrease AP-1 mediated transcription and that Gβγ localizes to promoters of over 700 genes in HEK 293 [26]. As Gβγ was capable of binding transcription factors, localized to promoters, and affected expression of fibrotic genes, we sought to examine whether Gβγ subunits interacted with a protein complex ubiquitously involved in transcription, initially focusing on RNA polymerase II (RNAPII). A co-immunoprecipitation time course experiment demonstrated that Ang II induced an interaction between endogenous Gβγ ($G\beta_{1\text{-}4}$; detected with a pan Gβ antibody) and Rpb1, the largest subunit of RNAPII, peaking 75 minutes post stimulation (Figure 1A,B). Cardiac fibroblasts express both angiotensin II type I and type II receptors. In order to distinguish which receptor induced the interaction in fibroblasts, the AT1R-specific antagonist losartan was used. Pretreatment of cells with losartan prior to Ang II treatment completely blocked the agonist-induced interaction, but preserved the basal interaction, suggesting that AT1R and not AT2R is responsible for mediating the interaction in cardiac fibroblasts (Supplemental Figure 2).

We validated this interaction following activation of a different endogenous receptor in a different cell line: carbachol stimulation of endogenous M3-muscarinic acetylcholine receptors (M3-MAChR) in HEK 293F cells (Supplemental Figure 3A,B). Under the same conditions, we observed no carbachol-dependent or basal interaction of Gβγ with the A194 subunit of RNAPI

(Supplemental Figure 3C). Immunoprecipitation of Rpb1 with two different antibodies also co-immunoprecipitated Gβ in an agonist-dependent manner (Supplemental Figure 3D). Additionally, we observed no basal or carbachol-dependent interaction of Rpb1 with Gαq/11 or ERK1/2 (Supplemental Figure 3E,F) suggesting that Gβγ was not in complex with these proteins when it was associated with RNAPII.

The localization of RNAPII is strictly nuclear, and although it has previously been described that different Gβγ isoforms are present in the nucleus [27-29], the mechanisms leading to entry of Gβγ into the nucleus remain unknown. Using subcellular fractionation following M3-MAChR activation in HEK 239 cells, we observed a net increase in the amount of Gβ in the nucleus and a net decrease in cytosolic levels 45 mins post stimulation (Supplemental Figure 4A). Inhibition of nuclear import using the importin-β inhibitor importazole also blocked M3-MAChR-dependent translocation of Gβ into the nucleus (Supplemental Figure 4B). In addition, recruitment of Gβ to RNAPII was blocked by importazole treatment, suggesting that upon M3-MAChR stimulation, nuclear import of Gβ is required for the interaction with RNAPII (Supplemental Figure 4C,D). Next, we determined whether nuclear localization of Gβγ is also necessary for the interaction to occur in response to Ang II in RNCF. The Ang II-stimulated interaction was ablated when nuclear import via importin-β was inhibited, suggesting again that Gβγ subunits must translocate to the nucleus for the interaction to occur (Figure 1C,D). Intriguingly, inhibition of importin-β under non-agonist stimulated conditions increased the basal interaction between Gβγ and Rpb1 (Figure 1D).

Specific roles for individual Gβ subunits in regulation of angiotensin II activated fibrotic response in rat neonatal cardiac fibroblasts

We next sought to determine the specificity of Gβ subunits interacting with Rpb1 in cardiac fibroblasts. Immunoprecipitation with a specific antibody for $G\beta_1$ revealed an increase in the amount of Rpb1 co-immunoprecipitated in response to Ang II treatment, whereas immunoprecipitation of $G\beta_2$ indicated a basal interaction with Rpb1 that is lost in response to Ang II treatment (Supplemental Figure 5). We next determined whether specific Gβ subunits were necessary to initiate signalling cascades immediately downstream of AT1R activation. Knockdown of $G\beta_1$ did not alter Ca^{2+} release downstream of stimulation with Ang II (8.1 ± 7.0% decrease, $p>0.05$; Figure 2A,B). However, knockdown of $G\beta_2$ resulted in a significant 31.6 ± 9% decrease in Ca^{2+} release (Figure 2A,B), suggesting that $G\beta_2$-containing Gβγ dimers mediate proximal signalling downstream of AT1R activation. Knockdown of $G\beta_2$ resulted in the loss of the Ang II-mediated increase in the interaction between Gβγ and Rbp1, likely a result of impaired signaling (Figure 2C,D). We also observed inhibition of the Ang II-induced RNAPII/Gβγ interaction upon knockdown of $G\beta_1$ even though $G\beta_1$ was not required for initiation of signalling downstream of AT1R. These results highlight the complex interplay between cell surface receptors and multiple Gβγ subunits in the basal and ligand-stimulated RNAPII/Gβγ interaction.

$G\beta_1$ preferentially interacts with the elongating form of RNAPII

Transcriptional activation through release of promoter-proximal pausing is thought to be particularly important for rapid responses to environmental stimuli [30]. Cdk7, a member of the general transcription factor TFIIH, and Cdk9, the kinase subunit of positive transcription elongation factor b (P-TEFb), are known to phosphorylate heptad repeats contained within the C-terminal domain of Rpb1 at serine positions 5 and 2, respectively (pSer5-Rpb1 and pSer2-Rpb1) [31]. The phosphorylation state of Rpb1 changes as RNAPII transcribes along the gene, with pSer5-Rpb1 more enriched at the 5' end and pSer2-Rpb1 at the 3' end. Serine 2 phosphorylation is a generally conserved mark of elongating RNAPII, which is enriched near the 3' ends of gene coding regions, and serves as a binding site for mRNA termination factors [31-33]. In order to assess how these differentially phosphorylated subtypes of Rpb1 interacted with Gβγ, we first assessed the effect of both Cdk7 and Cdk9 inhibition on our agonist-induced interaction, with the selective inhibitors THZ1 and iCdk9, respectively. Inhibition of Cdk7 abrogated the Ang II response (Figure 3A, Supplemental Figure 6A) while inhibition of Cdk9 resulted in a loss of both the basal and agonist-stimulated RNAP/Gβγ interaction (Figure 3B, Supplemental Figure 6B). Therefore, it would appear that this interaction involves the Ser2-phosphorylated, elongating form of RNAPII but that signal-dependent enhancement of the interaction occurs at an early post-initiation phase. Furthermore, we observed that Ang II treatment resulted in an increase in Gβγ interaction with pSer2-Rpb1 and no net change in the interactions with the pSer5-Rpb1 (Figure 3C,D, Supplemental Figure 6C,D). Interestingly, the effect of Ang II on levels of fibrotic genes in RNCFs was blocked by pretreatment with iCdk9 (data not shown).

Since the Ang II-mediated interaction between Gβγ and RNAPII was dependent on the phosphorylation status of Rpb1, we next assessed the localization patterns of $G\beta_1$ along fibrotic

genes by chromatin immunoprecipitation (ChIP)-qPCR. FLAG-tagged $G\beta_1$ was expressed in RNCFs and validated by western blot and immunofluorescence (Supplemental Figure 7). We chose five genes from the array described above (Akt1, Ctgf, Il10, Smad7, and Smad4). These genes were upregulated in response to Ang II and were affected by $G\beta_1$ knockdown (Supplemental Table 1). We assessed localization near the transcription start site (TSS), in the middle of the gene (exon) and at the 3' end (3' end) using primers targeting these specific regions (Figure 4A, Supplemental Table 2). We also examined the Akt1 promoter since we previously identified $G\beta_1$ promoter occupancy of Akt1 in a ChIP-on-chip experiment conducted in HEK 293 cells [34]. In all cases, $G\beta_1$ occupancy of the genes in question was increased by Ang II treatment, with a trend for greater occupancy near the 3' end (Figure 4B-E), consistent with the association of Gβγ with pSer2-Rpb1. Smad4 differed from the other four genes assessed, with $G\beta_1$ occupancy increasing only at the TSS in response to Ang II. This further suggests that Ang II stimulates the interaction of Gβγ primarily with the elongating form of RNAPII.

We next examined RNAPII and pSer2-Rpb1 occupancy at different regions along the genes (Figure5A) after $G\beta_1$ knockdown. In control samples, Ang II treatment caused either no change or a slight decrease in RNAPII occupancy (Figure 5B-F). $G\beta_1$ knockdown caused a decrease in basal RNAPII occupancy at all genes tested, with the exception of Smad4. Ang II treatment in these cells led to increased RNAPII occupancy at most sites tested within these genes (with the exception of Smad4, Figure 5J,K). This suggests that $G\beta_1$ negatively regulates RNAPII occupancy in response to Ang II. At Smad4 we observed an increase in basal occupancy and no effect (TSS) or a decrease (Exon) following Ang II treatment. The effect of $G\beta_1$

knockdown on pSer2-Rpb1 appears to varying greatly depending on the genomic loci investigated. We observed increases in basal occupancy with a decrease following Ang II, such as Akt1 TSS (Figure 5C). We also observed loci that had increased in pSer2-Rpb1 in response to Ang II following $G\beta_1$ knockdown, such as Ctgf 3' end (Figure 5E). Taken together, our data show that the interaction of $G\beta_1$ with RNAPII is regulated by kinases that control transcriptional initiation and processivity and that $G\beta_1$ is recruited to the chromatin along pro-fibrotic genes, modulating the transcriptional response to fibrotic stimuli.

Signals driving the Gβγ-RNAPII interaction are cell-specific

Finally, we examined the signalling events downstream of receptor signalling mediating the interaction between Gβγ and RNAPII in RNCFs (summarized in Figure 6) and in HEK 293F cells using a pharmacological approach. Our data suggest that the pathways responsible for induction of the interaction between Gβγ and RNAPII are cell-type- and pathway-specific. It has previously been demonstrated that AT1R couples to both Gq/11 and Gi/o G proteins [35]. FR900359 was used to inhibit Gαq/11 [36] and pertussis toxin (PTX) was used to inhibit Gαi/o. Although inhibition of either subfamily of G proteins did not completely abrogate the enhancement of the interaction by Ang II, and the basal interaction was increased when cells were treated with PTX, dual inhibition of both G proteins resulted in a loss of the interaction (Supplemental Figure 8A-C, Supplemental Figure 9A-C). As in the RNCFs, FR900359-mediated inhibition of Gαq/11 also resulted in a loss of the carbachol-induced interaction in HEK 293F cells (Supplemental Figures 10A and 11A). Further, CRISPR/Cas9-mediated knockout of Gαq/11/12/13 in HEK 293 cells also prevented a carbachol-mediated increase in the interaction

(Supplemental Figures 10B and 11B). Further, as with RNCFs, we noted that DRB, which inhibits both Cdk7 and Cdk9, also blocked the interaction between RNAPII and Gβγ in HEK 293F cells (data not shown) showing that events once again converged on regulation of transcriptional initiation and elongation.

However, except for the common events, the signalling pathways in neonatal rat cardiac fibroblasts and HEK 293F cells diverged substantially (for a summary, compare Figure 6 with Supplemental Figure 13). When we inhibited the activity of PLCβ, downstream of both Gq/11 and Gi/o (via Gβγ signalling) in RCNFs with U71322, the agonist-induced interaction between Gβγ and RNAPII was blocked, suggesting a pivotal role for PLCβ (Supplemental Figure 8D, Supplemental Figure 9D). Inhibition of PLCβ using U71322 in HEK 393 cells also blocked the carbachol-induced interaction although basal levels of the interaction were increased in the absence of receptor stimulation (Supplemental Figures 10C and 11C). Chelation of Ca^{2+} using BAPTA-AM in RCNFs also abrogated the agonist-induced interaction (Supplemental Figure 8E, Supplemental Figure 9E), as did inhibition of PKC with Gö6983 and inhibition of CaMKII with KN-93 (Supplemental Figure 8F,G, Supplemental Figure 9F,G). Interestingly, inhibition of MEK1 led to an increased basal interaction but an abrogation of the Ang II-induced interaction (Supplemental Figure 8H, Supplemental Figure 9H). Intriguingly, chelation of calcium using BAPTA-AM in HEK 293F cells also increased basal levels of the interaction and did not block the carbachol-induced interaction (Supplemental Figures 10D and 11D), suggesting a modulatory role for calcium for the interaction in HEK 293F cells rather than the direct role seen in neonatal rat cardiac fibroblasts. Similar effects, which differed from RNCFs, were observed upon inhibition of other protein kinases activated downstream of Gq/11-coupled GPCRs. For example, inhibition of PKC with Gö6983 and CamKII with KN-93 both increased basal levels

and did not block the carbachol-induced interaction between Gβ and Rpb1 (Supplemental Figures 10E,F and 11E,F). Calcium signaling has been previously described to be involved in the calcineurin- and PP1α-mediated disruption of the 7SK snRNP-HEXIM-P-TEFB complex, which leads to release of active P-TEFb and release of promoter-proximal RNAPII pausing [37]. Indeed, inhibition of calcineurin with cyclosporin A blocked the carbachol-mediated increase in interaction between Gβ and Rpb1, suggesting roles for this phosphatase in mediating the interaction upon M3-MAChR activation (Supplemental Figures 10G and 11G). Conversely, inhibition of calcineurin with cyclosporin A in rat neonatal cardiac fibroblasts increased the basal interaction and further amplified the Ang II-dependent increase in interaction (Supplemental Figure 12A,B). Inhibition of PP1α with calyculin A was attempted but not further pursued as this inhibitor proved to be too toxic for RNCFs (data not shown). Whether such cell-specific regulatory pathways are found in other cell types is an additional question that needs to be answered in further studies.

DISCUSSION

Here, we demonstrate for the first time a novel interaction between Gβγ and RNAPII that occurs in both transformed cell lines (HEK 293 cells) and in primary cells (rat neonatal cardiac fibroblasts). We show that Gβγ signalling is a critical regulator of the fibrotic response in RNCFs. Although a number of previous studies have focused on elucidating the significance of Gβ and Gγ subunit specificity for signalling proximal to GPCR activation (i.e., the regulation of effector activity downstream of receptor stimulation) (reviewed in [17]), our findings provide further insight regarding novel non-canonical roles of specific Gβγ dimers for more distal signalling in the nucleus, and in particular, the regulation of gene expression. The interaction of Gβγ and RNAPII is a significant addition to the expanding list of Gβγ interactors (reviewed in [17]), and our results suggest that this interaction is dependent on cellular context and is also signalling pathway-specific.

Regulatory pathways for gene expression downstream of Gα subunit activation have been extensively described [38], however, our understanding of how Gβγ and their complex signalling networks regulate gene expression remains rudimentary. Roles for Gβγ in the regulation of gene expression have primarily been described in the context of modulation and control of signalling pathways upon GPCR activation that ultimately converge on gene regulation (reviewed in [39]). Examples of this include the Gβγ-PI3K-Pax8 dependent transcription of sodium-iodide transporter and the modulation of interleukin-2 mRNA levels in CD4+ T-helper cells [40, 41]. Other studies have described more direct roles for Gβγ in gene expression regulation which include the relief of transcriptional repression exhibited by its interactions with AEBP1 [42] or the negative regulation of AP-1 through its interaction with c-Fos [26]. Furthermore, specific

roles for individual Gβγ subunits in regulating gene expression have only begun to be elucidated. For example, $G\beta_1\gamma_2$ was shown to interact with histone deacetylase 5 (HDAC5) resulting in the release of MEF2C and subsequent stimulation of transcriptional activity under conditions of α_{2A}-adrenergic receptor activation [43]. Another study demonstrated that $G\beta_2\gamma$ was translocated to the nucleus and interacted with MEF2 in response to stimulation of AT1R in a HEK 293 heterologous expression system [27]. Interestingly, these authors also identified an interaction between $G\beta_2\gamma$ and histone H2B and H4, which they suggested was due to transcription factor recruitment to the chromatin. Our data suggests this interaction is more ubiquitous than solely at locations where transcription factors bind *per se*, as we identified $G\beta_1$ occupancy along several different genes.

$G\beta_1$ was transiently recruited to Rpb1 following Ang II stimulation and this distinguishes it from other Gβ subunits. Selective inhibitors of Cdk7 and Cdk9 inhibited Ang II-mediated Gβγ recruitment to Rpb1 (Figure 3A,B), and our data suggest a preferential interaction of Gβγ with pSer2-Rpb1 upon AT1R activation (Figure 3C). Thus, our data suggests that $G\beta_1$ is a negative regulator of transcription elongation to a subset of fibrosis genes. Such a mechanism is well corroborated with the observation that knockdown of $G\beta_1$ results in upregulation of 19 genes implicated in fibrosis under basal conditions and 37 genes in response to Ang II, compared to 23 genes in control conditions (Supplemental Table 1). This is further shown by the localization pattern of $G\beta_1$ along fibrotic genes in response to Ang II. Following Ang II treatment, there was an increased recruitment of $G\beta_1$ towards the elongating RNAPII complex at the 3' end of several genes (Figure 4B-D). Further work is needed to determine whether $G\beta_1$ travels from the 5' end with RNAPII leading to accumulation at the 3' end or whether it is directly recruited to these

locations. $G\beta_1$ recruitment to Smad4 did not follow the same trend as we observed greater recruitment at the 5' end (Figure 4E). Interestingly, knockdown of $G\beta_1$ increased the basal transcription of Smad4 and attenuated the response to Ang II. This suggests distinct mechanisms for how $G\beta_1$ regulates RNAPII. Lastly, following Ang II treatment lengths resulting in the maximum amount of $G\beta\gamma$ interacting with Rpb1, we observed decreases in RNAPII occupancy along pro-fibrotic genes, such as Ctgf (Figure 5D). This negative regulation of RNAPII was released with $G\beta_1$ knockdown leading to an increase in RNAPII occupancy following Ang II. The distinctions between the time where $G\beta\gamma$ and RNAPII interact compared to the times where we measured gene expression may be sufficient to allow the cell to overcome the negative regulation imposed by $G\beta_1$.

With respect to $G\beta_2$-containing $G\beta\gamma$ dimers, we did not observe such dramatic changes to gene expression, with only 4 genes observed to be upregulated and 3 downregulated (Supplemental Table 1), with the rest of the genes analyzed following expression patterns similar to control conditions. Assessment of the roles of specific $G\beta\gamma$ that control second messenger release downstream of AT1R activation demonstrates that $G\beta_2$ knockdown results in a ~30% decrease in Ca^{2+} release, while $G\beta_1$ knockdown does not significantly alter Ca^{2+} release (Figure 2A,B). Our data suggest that role of $G\beta_2$ subunits in gene expression regulation are minimal, and that they are likely more important for proximal AT1R mediated signal transduction activation; evidence supporting this notion previous studies that have also shown $G\beta_2\gamma$ coupling to AT1R [27]. On the other hand, $G\beta_1$ containing $G\beta\gamma$ dimers are more important for direct regulation of RNAPII. Interestingly, knockdown of $G\beta_2$ did compromise Ang II-mediated interactions between $G\beta\gamma$ and RNAPII even though it had a limited role in the fibrotic response. This may

argue that it did not prevent the response *per se* but rather altered the kinetics of Gβγ/RNAPII interactions which then played out into different fibrotic responses over time. Further, the roles of specific Gγ subunits in mediating proximal signal transduction must also be considered as for other Gβγ effectors [34], and should be the subject of future studies. In any case, our data suggest that bulk targeting of Gβγ signalling in fibrosis and other diseases using compounds such as gallein may affect events in ways that are distinct from targeting subsets of Gβγ combinations [24, 44, 45].

Analysis of the signalling networks regulating the Gβγ/RNAPII interaction yields three main conclusions: (1) different GPCR signalling systems in distinct cell types show different kinetics of induction, (2) different signalling pathways downstream of GPCR activation act to both induce or modulate the interaction and (3) Gq-coupled GPCRs regulate the interaction in both cell types examined. Indeed, our results suggest elements of cell context are important when regarding the mechanism of action by which the Gβγ/RNAPII interaction is regulated. In rat neonatal cardiac fibroblasts, the interaction depended on a Gq-PLCβ-Ca^{2+}-CamKII/PKC/MEK-dependent pathway downstream of AT1R activation, whereas calcineurin acted as a basal negative regulator (summarized in Figure 6). The involvement of Ca^{2+}, PKC and ERK1/2 in the induction of the Gβγ/RNAPII interaction is supported by previous reports that demonstrate their involvement in Ang II-induced fibrosis [46, 47]. On the other hand, in HEK 293 cells, we observed that the interaction was reliant on a Gq-PLCβ-Ca^{2+}-calcineurin pathway in downstream of M3-MAChR activation, whereby PKC and CamKII both negatively regulate this interaction under basal conditions (summarized in Supplemental Figure 13). Irrespective of the different pathways taken to induce the Gβγ-Rpb1 interaction, these pathways converge on the activity of

Cdk9 and Cdk7 as inhibition of both of these kinases with iCdk9 or THZ1, respectively, resulted in the loss of both the carbachol-induced interaction in HEK 293 cells and Ang II-induced interaction in cardiac fibroblasts. Interestingly, a strong connection has been established between the control of transcriptional pausing and pathological cardiac remodelling, although most of that has been demonstrated in the cardiomyocyte [48-53]. RNAPII pausing has been demonstrated to prevent new transcription initiation, thus synchronizing transcriptional networks [54, 55]. Our results indicate that $G\beta_1$ acts to synchronize transcriptional networks in the cardiac fibroblast after RNAPII has been released from the paused state on a number of genes.

Taken together, the Gβγ/RNAPII interaction identifies a new role for Gβγ in modulating gene expression. Our studies highlight the complex interplay of different Gβγ dimers at the cell surface and in the nucleus initiated upon stimulation of different Gq-coupled receptors which involves different signalling intermediaries in different cell. Since $G\beta_1\gamma$ dimers have a unique role in controlling expression of fibrotic genes in cardiac fibroblasts, more selective pharmacological inhibition of the different Gβγ subunits may be an avenue for potential therapeutic intervention.

Acknowledgements

This work was supported by a grant from the Heart and Stroke Foundation of Canada to TEH and JCT, NSERC (to THE and PBSC) and CIHR (to TEH and JCT). We thank Asuka Inoue (Tohuku University) for the generous gift of the G protein knockout and parental cell lines. RM was supported by a scholarship from the Canadian Institutes of Health Research (CIHR). SMK and RM were supported by studentships from the McGill-CIHR Drug Development Training Program. JJT is supported by a CIHR Doctoral Scholarship and an award from the Healthy Brains for Healthy Lives at McGill University (supported by the Canada First Research Excellence Fund) and YS received a summer bursary from the Groupe d'étude des protéines membranaires (GEPROM). The authors thank Viviane Pagé for administrative and technical support.

FIGURE LEGENDS

Figure 1. Characterization of Gβγ-Rpb1 in rat neonatal cardiac fibroblasts – (A) Ang II stimulated interaction induction time course – assessment of the amount of Rpb1 co-immunoprecipitated with Gβ upon treatment of 1 μM Ang II treatment at the indicated time points in RNCFs. (B) Densitometry based quantification of Ang II interaction time course; data representative of two independent experiments. (C) Assessment of the necessity of Gβγ import into the nucleus for interaction to occur upon AT1R stimulation with Ang II. RNCF were pretreated for 1h with importazole prior to Ang II stimulation. Data representative of four independent experiments. (D) Densitometry based quantification of the Ang II induced interaction and the effect of nuclear import inhibition on interaction induction. Data is represented as mean ± S.E.M.

Figure 2. Gβ subunit specific effects on Ang II signalling and induction of Rpb1 interaction. **(A)** Raw traces of calcium release upon AT1R stimulation with Ang II under conditions of $G\beta_1$ and $G\beta_2$ knockdown. Data points are representative of mean ± S.E.M. of fluorescence ratios of 340/516 emission readings to 360/516 emissions recordings normalized to basal ratios, and of three independent experiments. (B) Area under the curve analysis of curves obtained in (A), * indicates $p<0.05$. (C) siRNA knockdown mediated assessment of specific Gβ subunits that interact with Rpb1 upon AT1R stimulation. RNCFs transfected with siRNA control, $G\beta_1$ or $G\beta_2$ for 72 hours, starved overnight and treated with Ang II for 75 minutes were assessed for interaction induction by co-IP and Western blots. (D) Densitometry based quantification of

knockdown experiments in (C); data is representative of mean ± S.E.M. of six independent experiments.

Figure 3. Functional analysis of Gβγ-Rpb1 interaction in rat neonatal cardiac fibroblasts – (A) Effect of Cdk7 inhibition with THZ1 on Ang II-induced Gβγ-Rpb1 interaction in RNCFs. Data is representative of three independent experiments. (B) Effect of Cdk9 inhibition with iCdk9 on Ang II-induced Gβγ-Rpb1 interaction in RNCFs. Data is representative of three independent experiments. Length of inhibitor pre-treatment is indicated on each respective subfigure, and assessment of interaction was performed via co-immunoprecipitation experiments coupled to western blot analysis. (C) Western plot for the amount of phosphorylated Serine 2 of the C-terminal domain heptad repeat of Rpb1 co-immunoprecipitated with Gβγ following Ang II treatment. Data is representative of five independent experiments. (D) Co-immunoprecipitation of Gβγ and phosphorylated Serine 5 of the C-terminal domain heptad repeat of Rpb1 in response to Ang II. Data is representative of six independent experiments. Data is represented as mean ± S.E.M. Corresponding quantification analyses of inhibitor co-IP experiments are depicted in Supplemental Figure 6.

Figure 4. **Chromatin immunoprecipitation-qPCR for FLAG-Gβ1 at various positions of genes from the qPCR array**. (A) Representative schematic of regions targeting on an average gene. % Input of FLAG-$G\beta_1$ at indicated regions along (B) Akt1, (C) Ctgf, (D) Il10, (E) Smad7, and (F) Smad4 following treatment with DMEM or 1 μM Ang II for 75 min. RNCF were transduced with AAV1-FLAG-$G\beta_1$ viral vector for 72h with a MOI of 10^3 and starved for 12h prior to treatment. Cells were fixed, lysed and sonicated after the indicated treatments, followed

by immunoprecipitation of the FLAG epitope or IgG. The % Input from IgG immunoprecipitation was subtracted from the FLAG immunoprecipitation for each condition. Data was normalized to the amount of yeast histone H2B pulled down by a species specific H2B antibody at the cdc2 promoter to account for different IP efficiencies between the samples. Data is represented as mean ± S.E.M. for six independent experiments. Unpaired t-test followed by Bonferroni correction was completed for each gene (*$p<0.05$).

Figure 5. **Chromatin immunoprecipitation for RNAPII and pSer2-Rpb1 following knockdown of $G\beta_1$ at various positions of fibrotic genes upregulated in response to Ang II**. (A) Schematic indicating regions of an average gene targeted with primers for ChIP-qPCR. Localization of Rpb1 and pSer2-Rpb1 was determined at indicated locations along (B-C) Akt1, (D-E) Ctgf, (F-G) Il10, (H-I) Smad7 and (J-K) Smad4. RNCFs were transfected with siRNA Control or siRNA $G\beta_1$ for 72h, starved for 12h and treated with Ang II for 75 min. The % input was normalized to the amount of spiked-in yeast chromatin pulled down as assessed by the % input of yeast cdc2 promoter to account for differences in IP efficiencies. The % input from IgG immunoprecipitation was subtracted from the FLAG immunoprecipitation for each condition. Data is represented as mean +/- SEM for four independent assays.

Figure 6. Summary of signalling mechanism regulating the agonist induced Gβγ interaction with Rpb1 in rat neonatal cardiac fibroblasts. Effect of indicated small molecule inhibitors on the Ang II induced interaction assessed by co-immunoprecipitation and western blot is shown on Supplemental Figure 8 and 9.

Supplemental Figure 1. Validation of RNAi knockdown of $G\beta_1$ and $G\beta_2$. (A,B) Validation of $G\beta_1$ and $G\beta_2$ mRNA (A) and protein (B) knockdown in RNCFs. Data in (A) are represented as fold change over control and is representative of 4 independent experiments; *** indicates $p<0.001$ and **** indicates $p<0.0001$.

Supplemental Figure 2. (A) Effect of AT1R antagonist (Losartan) pre-treatment on the Ang II-mediated interaction to demonstrate angiotensin receptor subtype specificity for the interaction in rat neonatal cardiac fibroblasts. (B) Densitometry based quantification of AT1R antagonist effect on Ang II-induced effect. Data is representative of three independent experiments.

Supplemental Figure 3. Supporting data for the induction of the Gβγ-Rpb1 interaction in HEK 293 cells – (A) Time-course analysis of the induction of the Gβγ-Rpb1 interaction – HEK 293 cells treated for the indicated times with 1 mM carbachol were subject to immunoprecipitation (IP) of Gβ from total lysates and the amount of Rpb1 co-immunoprecipitated (co-IP) was assessed by Western blot for each time point. Data is representative of three independent experiments. (B) Quantification of Gβγ-Rpb1 time-course IP. Densitometry analysis yielding values reflecting bands intensity that corresponding to amount of Rpb1 co-immunoprecipitated in each time point was normalized to the band intensity of the amount of Gβ immunoprecipitated to yield ratios of Rpb1 pulled down with Gβ. Resulting ratios were then normalized to the 0 mins treatment time point. Data is represented as mean ± S.E.M; ** indicates $p<0.01$, * indicates $p<0.05$. (C) Assessment of interaction between Gβ and Rpa194, the largest subunit of RNA polymerase I. Data represents analysis of a time course experiment blot performed as in Figure 1A. (D) Reverse-IP analysis of Rpb1 interacting with Gβ using two

different antibodies against Rpb1. Western blots are representative of at least two independent experiments. (E,F) Immunoprecipitation experiments demonstrating that carbachol treatment does not induce interaction of Rpb1 with Gαq nor ERK1/2 in HEK 293 cells, and also does not alter the amount of Gαq or ERK1/2 interacting with Gβγ under such conditions.

Supplemental Figure 4. Characterization of the interaction between Gβγ and Rpb1 in HEK 293 cells – (A) Quantitative analysis demonstrating decreases in Gβ content in the cytosol and accompanying increases in the nucleus upon carbachol treatment in HEK 293 cells. Cells treated with carbachol for increasing amounts of time were fractionated to yield cytosolic and nuclear fractions. Amounts of Gβ in each fraction were then assessed by western blot, upon which intensities from Gβ bands on blots were quantified using ImageJ. Data shown is representative of fold changes over 0 minutes treatment control and is indicative of a single experiment. (B) Effect of nuclear import inhibition with importazole on trafficking of Gβ to the nucleus. Cells pre-treated with 40 μM importazole and treated with carbachol for the indicated times were analyzed for Gβ distribution in the cytosol and nucleus as described in (A). (C) Densitometry based quantification of the carbachol induced interaction and the effect of nuclear import inhibition on interaction induction. Data is representative of three independent experiments for black bars, and two independent experiments for white bars (nuclear import inhibition conditions). (D) Subcellular fractionation-based assessment of the Gβγ-Rpb1 interaction assessed by co-IP.

Supplemental Figure 5. Assessment of specific Gβ subunits that interact with Rpb1 upon Ang II treatment in RNCFs. Gβ1 and Gβ2 were immunoprecipitated with subtype specific

antibodies from RNCF lysates treated with 1 μM Ang II for 75 minutes and the amount of Rpb1 pulled down with either Gβ was assessed.

Supplemental Figure 6. Quantitative analysis of the effect of inhibition of transcriptional regulators on Gβ with Rpb1 in neonatal rat cardiomyocytes. – (A-D) The relative quantities of Rpb1 co-immunoprecipitated with Gβ under different conditions depicted in Figure 3(A-D) were quantified using ImageJ and were normalized to amounts pulled down in DMSO/DMEM control conditions. Data shown is representative of between three to six independent co-immunoprecipitation and western blot experiments. Data is represented as fold change over respective controls and error bars represent S.E.M. * indicates $p<0.05$.

Supplemental Figure 7. Validation of Flag-tagged $G\beta_1$ in RNCF transduced with AAV_1-FLAG-$G\beta_1$. (A) Western blot with anti-FLAG M2 antibody to assess expression of FLAG-tagged $G\beta_1$ in RNCF following transduction with AAV1-FLAG-$G\beta_1$. (B) Immunofluorescence images of non-transduced and AAV1-FLAG-$G\beta_1$ transduced RNCF with anti-FLAG M2 antibody.

Supplemental Figure 8. Characterization of the mechanism through which Gβγ interacts with Rpb1 in rat neonatal cardiac fibroblasts – (A-H) Assessment of the effect of inhibition of signalling molecules and effectors implicated in AT1R signalling on the induction of the Gβγ-Rpb1 interaction in RNCFs. Concentrations of inhibitors and lengths of pre-treatment are indicated in each subfigure. 75 minutes of 1 μM Ang II treatment was used in all experiments shown to induce the interaction. Data shown is representative of between 3 and 6 independent

co-immunoprecipitation and western blot experiments. Corresponding quantification analyses of inhibitor co-IP experiments are depicted in Supplemental Figure 9.

Supplemental Figure 9. Quantitative analysis of the effect of inhibition of signalling molecules downstream of AT1R activation – (A-H) The relative quantities of Rpb1 co-immunoprecipitated with Gβ under different conditions depicted in Supplemental Figure 8 were quantified using ImageJ and were normalized to amounts pulled down in DMSO/DMEM control conditions. Data shown is representative of between 3 and 6 independent co-immunoprecipitation and western blot experiments. Data is represented as fold change over respective controls and error bars represent S.E.M. * indicates $p<0.05$, ** indicates $p<0.01$.

Supplemental Figure 10. Analysis of the mechanism through which the carbachol-induced Gβγ interaction occurs in HEK 293 cells – (A-G) HEK 293 cells starved for 10-12 hours in DMEM without FBS were pre-treated with the indicated inhibitors against different proteins for the indicated times. Cells were then treated with carbachol for 45 minutes and analysis of effector inhibition on of the amount of Rpb1 co-immunoprecipitated with Gβ was assessed by western blot. Data is representative of at least 3 independent experiments. The associated quantifications of the co-IPs are represented on Supplemental Figure 11.

Supplemental Figure 11. Quantitative analysis of the effect of inhibition of signalling molecules downstream of muscarinic acetylcholinergic receptor activation in HEK 293 cells – (A-G) The relative quantities of Rpb1 co-immunoprecipitated with Gβ under different conditions depicted in Supplemental Figure 10 were quantified using ImageJ and were

normalized to amounts pulled down in DMSO/DMEM control conditions. Data shown is representative of between 3 and 6 independent co-immunoprecipitation and western blot experiments. Data is represented as fold change over respective controls and error bars represent S.E.M. * indicates $p<0.05$.

Supplemental Figure 12. Assessment of effect of calcineurin on the Ang II-induced Gβγ and Rpb1 interaction in RNCF. (A) RNFC were pretreated with cyclosporin A for 1 h followed by a 75 min treatment with Ang II. Analysis of the effect of calcineurin inhibition on the amount of Rpb1 co-immunoprecipitated with Gβ was assessed by western blot. (B) Densitometry based analysis of calcineurin inhibition effect on interaction. Data is represented as mean ± S.E.M for four independent experiments.

Supplemental Figure 13. Summary of signalling mechanisms regulating muscarinic receptor-induced Gβγ interaction with Rpb1 in HEK 293 cells. Effect of indicated small molecule inhibitors on the carbachol-induced interaction assessed by co-immunoprecipitation and western blot is shown on Supplemental Figure 10 and 11.

Supplemental Table 1. Complete table of fibrosis qPCR array results – Table portrays complete list of observed changes on gene expression under conditions of siRNA control, siRNA $G\beta_1$ or siRNA $G\beta_2$ with vehicle or Ang II treatment. Fold changes over siRNA control/DMEM conditions are listed in rows next to each gene. Boxes highlighted in green indicate trends for upregulation, boxes highlighted in yellow indicate significant upregulation compared to

respective control, boxes in red indicate trends for downregulation, while boxes in blue indicate genes significantly downregulated compared to respective control. Data is represented as fold change over control calculated from three independent samples for each condition run on each replicate's own PCR array plate. Repeated-measure one-way ANOVA followed by Bonferroni's post-hoc analysis on selected comparisons was completed.

Supplemental Table 2. List of RT-qPCR primers used for validation of $G\beta_1$ and $G\beta_2$ knockdown and ChIP-qPCR in rat neonatal cardiac fibroblasts – Forward and reverse primers were used at concentrations of 300 nM for each qPCR reaction. Primer sequences were designed using NCBI's Primer-BLAST tool and validated by analysis of standard curve qPCR assays performed in-house.

METHODS

Reagents – Carbachol, angiotensin II, BAPTA-AM, KN-93, Gö6983, PTX, U0126, calyculin A, cyclosporin A, TRI reagent, isopropyl thiogalactopyranoside (IPTG), protease inhibitor cocktail, triton X-100, bovine serum albumin, ethylenediaminetetraacetic acid (EDTA), 70% NP-40 (Tergitol), sodium deoxycholate, magnesium chloride, anti-rabbit IgG (whole molecule)-agarose antibody, anti-mouse IgG (whole molecule)-agarose antibody, goat anti-rabbit IgG (whole molecule) conjugated to peroxidase secondary antibody, goat anti-mouse IgG (Fab specific) conjugated to peroxidase secondary antibody, anti-FLAG M2 antibody, rabbit IgG and polybrene were all purchased from Sigma-Aldrich Corp. (St. Louis, MO, USA). U71322 pan-PKC inhibitor was purchased from Biomol International (Plymouth Meeting, PA, USA). Lysozyme (from hen

egg white) and phenylmethylsulfonyl fluoride (PMSF) were purchased from Roche Applied Sciences (Laval, QC, Canada). Ethylene glycol bis (2-aminooethyl ether) N,N,N',N' tetraacetic acid (EGTA) and HEPES were purchased from BioShop (Burlington, ON, Canada). Sodium chloride, glutathione reduced, dithiothreitol (DTT) and Dynabead protein G were purchased from Fisher Scientific (Ottawa, ON, Canada). Dulbecco's modified Eagle's medium (DMEM) supplemented with 4.5 g/L glucose, L-glutamine and phenol red, low glucose DMEM supplemented with 1.0 g/L glucose, L-glutamine and phenol red, Penicillin/Streptomycin solution, Tris base buffer, ampicillin sodium salt, and fetal bovine serum were purchased from Wisent (St. Bruno, QC, Canada). Glutathione sepharose 4B GST beads were purchased from GE Healthcare (Mississauga, ON, Canada). Lipofectamine 2000 and Alexa Fluor 488 goat anti-mouse IgG was purchased Enhanced chemiluminescence (ECL) Plus reagent was purchased from Perkin Elmer (Woodbridge, ON, Canada). Moloney murine leukemia virus reverse transcriptase (MMLV-RT) enzyme and recombinant RNasin ribonuclease inhibitor were purchased from Promega (Madison, WI, USA). Evagreen 2X qPCR mastermix was purchased from Applied Biological Materials Inc. (Vancouver, BC, Canada) and iQ SYBR Green Supermix was purchased from Bio-Rad Laboratories (Mississauga, ON, Canada). Anti-Gβ1-4 (T-20) antibody, anti-RNA Polymerase I Rpa194 (N-16) antibody, anti-ERK1/2 antibody and anti-Gαq antibody was purchased from Santa Cruz Biotechnology, Inc. (Dallas, TX, USA). Anti-RNA polymerase II clone CTD4H8 (Rpb1) antibody, anti-RNA polymerase II subunit B1 (phospho CTD Ser-2) clone 3E10 antibody and anti-RNA polymerase II subunit B1 (phospho CTD Ser-5) clone 3E8 antibody were purchased from EMD Millipore (Temecula, CA, USA). Anti-GST antibody was purchased from Rockland Immunochemicals (Limerick, PA, USA). Anti-*Schizosaccharomyces pombe* histone H2B (ab188271) antibody was purchased from Abcam Inc.

(Toronto, ON, Canada). Polyclonal anti-$G\beta_1$ and anti-$G\beta_2$ were a generous gift of Professor Ron Taussig (UT Southwestern). Ethynyl uridine was synthesized by Zamboni Chemical Solutions (Montréal, QC, Canada). THZ1 was a gift from Nathanael S. Gray (Harvard University) and iCdk9 was a gift from James Sutton (Novartis).

Tissue culture, transfection and treatments – Human embryonic kidney 293 (HEK 293), HEK 293T cells and CRISPR-Cas9 mediated $\Delta G\alpha_{q/11/12/13}$ knockout HEK 293 cells (quadKO cells) [56], a generous gift from Dr. Asuka Inoue (Tohuku University, Sendai, Japan), were grown at 37°C in 5% CO_2 in high glucose DMEM supplemented with 5% (v/v) fetal bovine serum and 1% (v/v) penicillin/streptomycin (P/S). HEK 293 cells were transiently transfected with FLAG-Gβ1-5 using Lipofectamine 2000 as per the manufacturer's recommendations and as previously described. Primary rat neonatal cardiac fibroblasts were isolated as previously described with minor modifications [57]. Briefly, hearts from 1-3 one-day old rat pups were cut into 2-3 pieces and trypsinized overnight at 4°C with gentle agitation. The next morning, trypsin was neutralized by the addition of fibroblast growth medium (DMEM supplemented with 7% FBS (v/v) and 1% P/S (v/v)) and cells were subsequently treated with collagenase five times for ~1 min in a 37°C water bath. Cells were filtered through a 40 μm filter, pelleted, resuspended in HBSS and pelleted again at $400g^{-1}$ for 5 mins at 4°C. The resulting cell pellet was resuspended in a total of 40 mL of fibroblast growth medium and plated in 100 mm plates and grown at 37°C in 5% CO_2 for 75min. After pre-plating, media was removed from the plates to minimize cardiomyocyte attachment, cells were washed once with fibroblast media, and then grown for 48 hours at 37°C in 5% CO_2. Two days post plating, cells were trypsinized and seeded at a density of $8.3x10^3$ cells/cm^2 on required plate in fibroblast growth medium for 48h. For treatment of

HEK 293 cells, quadKO cells or RNCFs, cells were starved in DMEM (with no FBS and no P/S) overnight for between 10-12 hours and subsequently treated with pathway inhibitors, 1 mM carbachol or 1 μM Ang II for the treatment lengths indicated in the various assays listed below.

RT-qPCR – Reverse transcription of RNA isolated from rat neonatal cardiac fibroblasts was performed using a protocol previously described [34]. Briefly, cells plated in 100 mm dishes were lysed in TRI reagent and RNA was extracted using a protocol adapted from Ambion (Burlington, ON, Canada). Reverse transcription was performed on 1 μg of total RNA using an MMLV-RT platform according to the manufacturer's protocol. Subsequent qPCR analysis on $G\beta_1$ and $G\beta_2$ transcripts was performed with Evagreen Dye qPCR master-mixes using a Corbett Rotorgene 6000 thermocycler. mRNA expression data were normalized to housekeeping transcripts for U6 snRNA. Ct values obtained were analyzed to calculate fold change over respective control values using the $2^{-\Delta\Delta Ct}$ method. Primer sequences for all primers used are listed in Supplemental Table 2.

Nuclear isolation – Nuclei from HEK293 cells were isolated as previously described [28]. Briefly, cells seeded in T175 flasks were treated as indicated, washed three times with 1X PBS (137 mM NaCl, 2.7 mM KCl, 10 mM Na_2HPO_4, 1.8 mM KH_2PO_4), and harvested in 1X PBS by centrifugation. Pelleted cells were lysed in lysis buffer (320mM sucrose, 10 mM HEPES, 5 mM $MgCl_2$, 1 mM DTT, 1 mM PMSF, 1% Triton X-100), added gently on top of a high-sucrose buffer (1.8 M sucrose, 10 mM HEPES, 5 mM $MgCl_2$, 1 mM DTT, 1 mM PMSF), and centrifuged at 4600 g^{-1} for 30 minutes at 4°C, separating unlysed nuclei from the cytosolic fraction. Pelleted nuclei were then resuspended in resuspension buffer (320 mM sucrose, 10 mM

HEPES, 5 mM $MgCl_2$, 1 mM DTT, 1 mM PMSF), pelleted at 300 g^{-1} for 5 minutes and subsequently lysed in 1X RIPA buffer.

Immunoprecipitation and western blotting – Immunoprecipitation (IP) assays of Gβ and Rpb1 pull downs were performed as previously described, with minor alterations [26]. Treated HEK293 cells and RNCFs lysed in 1X RIPA (1% NP-40, 50 mM Tris-HCl pH 7.4, 150 mM NaCl, 1 mM EDTA, 1 mM EGTA, 0.1% SDS, 0.5% sodium deoxycholate) were first quantified with Bradford assay, upon which 500 µg of lysates were precleared with 15 µl of anti-rabbit IgG-agarose beads. Precleared lysates were then incubated with 1 µg anti-$G\beta_{1-4}$ or 2 µg of anti-Rpb1 overnight at 4°C with end-over mixing. The next day, 40 µl of washed beads were added to each lysate/antibody mixture, incubated for 3.5 hours at 4°C with end-over mixing, and then beads were washed 3X with 1X RIPA. Proteins were then eluted off the beads by the addition of 4X Laemmli buffer followed by denaturation at 65°C. Protein immunoprecipitation and co-IP was then assessed by western blot as previously described [34]. Resulting western blot images were then quantified using ImageJ 1.48v and analyzed in GraphPad Prism 6.0c software.

Rat Fibrosis qPCR arrays – Fibrosis qPCR arrays were performed as per the manufacturer's protocols (Qiagen, Toronto, ON, Canada). Briefly, 0.5 µg of isolated total RNA (A_{260}:A_{230} ratios greater than 1.7, A_{260}:A_{280} ratios between 1.8 and 2.0) from siRNA transfected and vehicle/Ang II treated rat neonatal cardiac fibroblasts were subject to genomic DNA elimination using mixes supplied with the array kit for 5 mins at 42°C. DNA eliminated RNA was then subject to reverse transcription reactions using RT^2 First Strand Kits with protocols according to the manufacturer's instructions. Resulting cDNA mixes were then mixed with RT2 SYBR Green

mastermixes and subsequently dispensed in wells of a 96-well plate containing pre-loaded lyophilized primers provided by the manufacturer. qPCR reactions were then run on an Applied Biosystems ViiA 7 thermocycler according to the manufacturers cycle recommendations. Each sample was run on separate individual 96 well plates and Ct values for each gene assessed were collected and analyzed; Ct values greater than 35 were eliminated from the overall analysis. A list of all the genes whose expressions were detected can be found at https://www.qiagen.com/ca/shop/pcr/primer-sets/rt2-profiler-pcr-arrays?catno=PARN-120Z#geneglobe. mRNA expression data were normalized to levels of two housekeeping genes contained on each plate – Ldha1 and Hprt.

AAV Production and Transduction of RNCF – pcDNA3.1+-FLAG-Gβ_1 and pcDNA3.1+-FLAG-Gβ_2 were obtained from UMR cDNA Resource (www.cdna.org). Individual FLAG-Gβ was PCR amplified from pcDNA3.1+ and BamHI and EcoRI restrictions sites added to the 5' and 3' end, respectively. These restrictions sites were used to insert each FLAG-Gβ into the pAAV-CAG plasmid. Adeno-associated viruses were produced as previously described [58]. Cells were transduced with AAV1-FLAG-Gβ_1 (MOI of 10^3) in DMEM -/- for 6h and the media changed to fibroblast growth media for another 24h. At this point, the cells were trypsinized and plated as we previously described. Expression was determined by western blot and immunofluorescence. For immunofluorescence, cells were fixed with 4% PFA for 10 min at 4°C, blocked with 10% horse serum in PBS for 1h at RT, followed by overnight incubation with primary anti-FLAG M2 antibody in 10% horse serum/PBS at 4°C. This was followed by incubation with anti-mouse Alexa 488 for 1h at room temperature in 10% horse serum/PBS, 30

min incubation with cell mask dye (1 μg/μL), and 10 min with Hoechst dye (1 μg/μL). The stained RNCF were imaged with an Opera Phenix high content imaging system.

Chromatin Immunoprecipitation-qPCR – Chromatin immunoprecipitation in RNCF was performed as previously described, with minor modifications [59]. RNCFs were plated in 15 cm dishes at $1.25x10^6$ cells per dish and cultured as previously described. Following the indicated treatment, RNCFs were fixed with 1% formaldehyde in DMEM low glucose for 10 min at room temperature with light shaking. Crosslinking was quenched by the addition of glycine to a final concentration of 0.125M and continued shaking for 5 min at room temperature. RNCFs were placed on ice following crosslinking, washed 1x with cold PBS, and scraped into PBS with 1mM PMSF. Cells were pelleted at 800 g^{-1} for 5 min, followed by resuspension in cell lysis buffer (10 mM Tris-HCl pH 8.0, 10 mM EDTA, 0.5 mM EGTA, 0.25% Triton X-100, 1 mM PMSF, 1x protease inhibitor cocktail) and incubate for 10 min at 4°C on a rocker. Nuclei were pelleted at 800 g^{-1} for 5 min and resuspended in nuclei lysis buffer (50 mM Tris-HCl pH 8.0, 10 mM EDTA, 1% SDS, 1 mM PMSF, 1x protease inhibitor cocktail). Nuclei were incubated for 15 min on ice then sonicated with a BioRuptor (15 cycles, 30sec on/off, high power) and spun for 10 min at 14 000 g^{-1} to remove cellular debris. An aliquot of chromatin was taken and reverse crosslinked by incubation at 65°C overnight, followed by 0.05 mg/mL RNAse treatment for 15 min at 37°C, 0.2 mg/mL proteinase K treatment at 42°C for 90 min. Protein was removed by phenol/chloroform extraction, and DNA was incubated at -80°C for 1 h with 0.3M sodium acetate pH 5.2, 2.5 volumes of 100% ethanol, and 20 mg of glycogen. Following incubating, DNA was centrifuged at 14 000 g^{-1} for 10 min, washed with 70% ethanol, resuspended in water, and quantified with a NanoDrop. Following quantification of chromatin, 10 μg of chromatin

(FLAG IPs) or 5 μg (RNAPII and pSer2-Rpb1 IPs) was diluted 9x with dilution buffer (16.7 mM Tris-HCl pH 8.0, 1.2 mM EDTA, 167 mM NaCl, 0.01% SDS, 1.1% Triton X-100, 1x protease inhibitor cocktail) and anti-FLAG M2 antibody (2 μg), anti-Rpb1 (8WG16) antibody (2 μg), anti-pSer2-Rbp1 (2 μg), or equivalent IgG was added to respective IPs. Schizosaccharomyces pombe yeast chromatin for spike-in was obtained as previously described [60]. For spike-in, 5 μg of yeast chromatin was added to each IP alongside an anti- *Schizosaccharomyces pombe* H2B antibody. Antibody and chromatin was incubated at 4°C overnight on a shaker, 15 μL of DynaBeads was added the following morning for 4h. Beads were washed 2x with low salt buffer (20 mM Tris-HCl pH 8.0, 2 mM EDTA, 150 mM NaCl, 0.1% SDS, 1% Triton X-100), 2x with high salt buffer (20 mM Tris-HCl pH 8.0, 2 mM EDTA, 500 mM NaCl, 0.1% SDS, 1% Triton X-100), 1x with LiCl buffer (10 mM Tris-HCl pH 8.0, 1 mM EDTA, 0.25M LiCl, 1% NP-40, 1% deoxycholate), 1x with TE buffer (10mM Tris-HCl pH 8.0, 1 mM EDTA) at 4°C. Chromatin was eluted with elution buffer (200 mM NaCl, 1% SDS) and reverse crosslinked overnight at 65°C, followed by treatment with 0.2 mg/mL of proteinase K for 2h at 37°C. DNA was further cleaned up as previously described for chromatin quantification. Localization was assessed by qPCR with primers for specific genomic loci (Supplemental table 2). All qPCR reactions were performed using a Bio-Rad 1000 Series Thermal Cycling CFX96 Optical Reaction module and iQ SYBR Green Supermix. % Input of IgG control for each treatment was subtracted off of the respective IP, followed by normalization to the % Input yeast cdc2 of each IP to account for differences in IP efficiencies.

Statistical Analysis – Statistical tests were performed using GraphPad Prism 6.0c software. For analysis on quantifications of immunoprecipitation experiments, one-way analysis of variance

(ANOVA) followed by post-hoc Dunnett's correction was used on raw quantifications of western blot bands and comparisons were made to vehicle-vehicle conditions. For assessment of Ca^{2+} release using Fura-2 AM based assays, one way ANOVA followed by Dunnett's correction was used on areas under curves derived from Ca^{2+} release – time graphs and comparisons were made back to either siRNA control conditions or vehicle/vehicle conditions. For fibrosis qPCR arrays, repeated measures one way ANOVA followed by Bonferroni's post-hoc analysis was used to determine differences in gene expression with all comparisons made to respective siRNA control or no treatment conditions within siRNA conditions. For validation of $G\beta_1$ and $G\beta_2$ knockdown in cardiac fibroblasts, fold changes over siRNA control were compared to siRNA control using Student's t-tests. For FLAG-$G\beta_1$ ChIP-qPCR, unpaired Student t-tests with a Bonferroni post-hoc correction were completed. For RNAPII and pSer2-Rpb1 ChIP-qPCR, a two-way ANOVA followed by select comparisons with Bonferroni post-hoc correction was completed. Comparisons that resulted with p values that were $p<0.05$ were considered significant. All results are expressed as mean ± S.E.M and data are represented as pooled experiments whose sample sizes are indicated in figure legends.

REFERENCES

1. Weber, K.T., et al., *Regression of Established Cardiac Fibrosis in Hypertensive Heart Disease.* Am J Hypertens, 2017. **30**(11): p. 1049-1052.
2. Weber, K.T., et al., *Myofibroblast-mediated mechanisms of pathological remodelling of the heart.* Nat Rev Cardiol, 2013. **10**(1): p. 15-26.
3. Gonzalez, A., et al., *Myocardial Interstitial Fibrosis in Heart Failure: Biological and Translational Perspectives.* J Am Coll Cardiol, 2018. **71**(15): p. 1696-1706.
4. Fu, X., et al., *Specialized fibroblast differentiated states underlie scar formation in the infarcted mouse heart.* J Clin Invest, 2018. **128**(5): p. 2127-2143.
5. Lynch, M.D. and F.M. Watt, *Fibroblast heterogeneity: implications for human disease.* J Clin Invest, 2018. **128**(1): p. 26-35.
6. Travers, J.G., et al., *Cardiac Fibrosis: The Fibroblast Awakens.* Circ Res, 2016. **118**(6): p. 1021-40.
7. Thannickal, V.J., et al., *Myofibroblast Differentiation by Transforming Growth Factor-β1 Is Dependent on Cell Adhesion and Integrin Signaling via Focal Adhesion Kinase.* Journal of Biological Chemistry, 2003. **278**(14): p. 12384-12389.
8. Macconi, D., G. Remuzzi, and A. Benigni, *Key fibrogenic mediators: old players. Renin-angiotensin system.* Kidney Int Suppl (2011), 2014. **4**(1): p. 58-64.
9. Leask, A., *TGFβ, cardiac fibroblasts, and the fibrotic response.* Cardiovascular Research, 2007. **74**(2): p. 207-212.
10. Lee, A.A., et al., *Angiotensin II stimulates the autocrine production of transforming growth factor-β1 in adult rat cardiac fibroblasts.* Journal of Molecular and Cellular Cardiology, 1995. **27**(10): p. 2347-2357.
11. Campbell, S.E. and L.C. Katwa, *Angiotensin II Stimulated Expression of Transforming Growth Factor-β1in Cardiac Fibroblasts and Myofibroblasts.* Journal of Molecular and Cellular Cardiology, 1997. **29**(7): p. 1947-1958.
12. Cheng, T.-H., et al., *Involvement of reactive oxygen species in angiotensin II-induced endothelin-1 gene expression in rat cardiac fibroblasts.* Journal of the American College of Cardiology, 2003. **42**(10): p. 1845-1854.
13. Ahmed, M.S., et al., *Connective tissue growth factor—a novel mediator of angiotensin II-stimulated cardiac fibroblast activation in heart failure in rats.* Journal of Molecular and Cellular Cardiology, 2004. **36**(3): p. 393-404.
14. Gao, X., et al., *Angiotensin II increases collagen I expression via transforming growth factor-beta1 and extracellular signal-regulated kinase in cardiac fibroblasts.* European Journal of Pharmacology, 2009. **606**(1–3): p. 115-120.
15. Valiente-Alandi, I., et al., *Inhibiting Fibronectin Attenuates Fibrosis and Improves Cardiac Function in a Model of Heart Failure.* Circulation, 2018.
16. Weber, K.T. and J. Diez, *Targeting the Cardiac Myofibroblast Secretome to Treat Myocardial Fibrosis in Heart Failure.* Circ Heart Fail, 2016. **9**(8).
17. Khan, S.M., et al., *The Expanding Roles of Gβγ Subunits in G Protein–Coupled Receptor Signaling and Drug Action.* Pharmacological Reviews, 2013. **65**(2): p. 545-577.

18. Dupré DJ, R.M., Rebois RV, Hébert TE, *The role of Gβγ subunits in the organization, assembly and function of GPCR signaling complexes.* Annu. Rev. Pharmacol. Toxicol., 2009. **49**: p. 31-56.
19. Smrcka, A.V., *G protein βγ subunits: central mediators of G protein-coupled receptor signaling.* Cell Mol Life Sci, 2008. **65**.
20. Campden, R., N. Audet, and T.E. Hébert, *Nuclear G Protein Signaling: New Tricks for Old Dogs.* Journal of Cardiovascular Pharmacology, 2015. **65**(2): p. 110-122.
21. van Berlo, J.H., M. Maillet, and J.D. Molkentin, *Signaling effectors underlying pathologic growth and remodeling of the heart.* J Clin Invest, 2013. **123**(1): p. 37-45.
22. Kamal, F.A., et al., *G Protein-Coupled Receptor-G-Protein betagamma-Subunit Signaling Mediates Renal Dysfunction and Fibrosis in Heart Failure.* J Am Soc Nephrol, 2017. **28**(1): p. 197-208.
23. Travers, J.G., et al., *Pharmacological and Activated Fibroblast Targeting of Gbetagamma-GRK2 After Myocardial Ischemia Attenuates Heart Failure Progression.* J Am Coll Cardiol, 2017. **70**(8): p. 958-971.
24. Kamal, F.A., A.V. Smrcka, and B.C. Blaxall, *Taking the heart failure battle inside the cell: small molecule targeting of Gbetagamma subunits.* J Mol Cell Cardiol, 2011. **51**(4): p. 462-7.
25. Casey, L.M., et al., *Small molecule disruption of G beta gamma signaling inhibits the progression of heart failure.* Circ Res, 2010. **107**(4): p. 532-9.
26. Robitaille, M., et al., *Gβγ is a negative regulator of AP-1 mediated transcription.* Cell Signal, 2010. **22**(8): p. 1254-66.
27. Bhatnagar, A., et al., *Interaction of G-protein betagamma complex with chromatin modulates GPCR-dependent gene regulation.* PLoS One, 2013. **8**(1): p. e52689.
28. Campden, R., et al., *Tandem Affinity Purification to Identify Cytosolic and Nuclear Gβγ-Interacting Proteins*, in *Nuclear G-Protein Coupled Receptors*, B.G. Allen and T.E. Hébert, Editors. 2015, Springer New York. p. 161-184.
29. Zhang, J.H., et al., *Nuclear localization of G protein beta 5 and regulator of G protein signaling 7 in neurons and brain.* J Biol Chem, 2001. **276**(13): p. 10284-9.
30. Liu, X., W.L. Kraus, and X. Bai, *Ready, pause, go: regulation of RNA polymerase II pausing and release by cellular signaling pathways.* Trends Biochem Sci, 2015. **40**(9): p. 516-25.
31. Zhou, Q., T. Li, and D.H. Price, *RNA polymerase II elongation control.* Annu Rev Biochem, 2012. **81**: p. 119-43.
32. Komarnitsky, P., E.J. Cho, and S. Buratowski, *Different phosphorylated forms of RNA polymerase II and associated mRNA processing factors during transcription.* Genes Dev, 2000. **14**(19): p. 2452-60.
33. Morris, D.P., G.A. Michelotti, and D.A. Schwinn, *Evidence that phosphorylation of the RNA polymerase II carboxyl-terminal repeats is similar in yeast and humans.* J Biol Chem, 2005. **280**(36): p. 31368-77.
34. Khan, S.M., et al., *Gβ4γ1 as a modulator of M3 muscarinic receptor signalling and novel roles of Gβ1 subunits in the modulation of cellular signalling.* Cellular Signalling, 2015. **27**(8): p. 1597-1608.
35. Sauliere, A., et al., *Deciphering biased-agonism complexity reveals a new active AT1 receptor entity.* Nat Chem Biol, 2012. **8**(7): p. 622-30.

36. Schrage, R., et al., *The experimental power of FR900359 to study Gq-regulated biological processes.* Nat Commun, 2015. **6**: p. 10156.
37. Chen, R., et al., *PP2B and PP1alpha cooperatively disrupt 7SK snRNP to release P-TEFb for transcription in response to Ca2+ signaling.* Genes Dev, 2008. **22**(10): p. 1356-68.
38. Ho, M.K.C., et al., *Regulation of Transcription Factors by Heterotrimeric G Proteins.* Current Molecular Pharmacology, 2009. **2**(1): p. 19-31.
39. Dorsam, R.T. and J.S. Gutkind, *G-protein-coupled receptors and cancer.* Nat Rev Cancer, 2007. **7**(2): p. 79-94.
40. Zaballos, M.A., B. Garcia, and P. Santisteban, *Gβγ Dimers Released in Response to Thyrotropin Activate Phosphoinositide 3-Kinase and Regulate Gene Expression in Thyroid Cells.* Molecular Endocrinology, 2008. **22**(5): p. 1183-1199.
41. Yost, E.A., et al., *Inhibition of G-Protein βγ Signaling Enhances T Cell Receptor-Stimulated Interleukin 2 Transcription in CD4⁺ T Helper Cells.* PLoS ONE, 2015. **10**(1): p. e0116575.
42. Park, J.G., et al., *Transcriptional regulation by the gamma5 subunit of a heterotrimeric G protein during adipogenesis.* Embo J, 1999. **18**(14): p. 4004-12.
43. Spiegelberg, B.D. and H.E. Hamm, *Gβγ binds histone deacetylase 5 (HDAC5) and inhibits its transcriptional co-repression activity.* J Biol Chem, 2005. **280**(50): p. 41769-76.
44. Lin, Y. and A.V. Smrcka, *Understanding molecular recognition by G protein betagamma subunits on the path to pharmacological targeting.* Mol Pharmacol, 2011. **80**(4): p. 551-7.
45. Smrcka, A.V., D.M. Lehmann, and A.L. Dessal, *G protein betagamma subunits as targets for small molecule therapeutic development.* Comb Chem High Throughput Screen, 2008. **11**(5): p. 382-95.
46. Chintalgattu, V. and L.C. Katwa, *Role of protein kinase C-δ in angiotensin II induced cardiac fibrosis.* Biochemical and Biophysical Research Communications, 2009. **386**(4): p. 612-616.
47. Olson, E.R., et al., *Angiotensin II-Induced Extracellular Signal-Regulated Kinase 1/2 Activation Is Mediated by Protein Kinase Cδ and Intracellular Calcium in Adult Rat Cardiac Fibroblasts.* Hypertension, 2008. **51**(3): p. 704-711.
48. Yang, J., B. Tian, and A.R. Brasier, *Targeting Chromatin Remodeling in Inflammation and Fibrosis.* Adv Protein Chem Struct Biol, 2017. **107**: p. 1-36.
49. Sayed, D., et al., *Transcriptional regulation patterns revealed by high resolution chromatin immunoprecipitation during cardiac hypertrophy.* J Biol Chem, 2013. **288**(4): p. 2546-58.
50. Anand, P., et al., *BET bromodomains mediate transcriptional pause release in heart failure.* Cell, 2013. **154**(3): p. 569-82.
51. Duan, Q., et al., *BET bromodomain inhibition suppresses innate inflammatory and profibrotic transcriptional networks in heart failure.* Sci Transl Med, 2017. **9**(390).
52. Stratton, M.S., et al., *Signal-Dependent Recruitment of BRD4 to Cardiomyocyte Super-Enhancers Is Suppressed by a MicroRNA.* Cell Rep, 2016. **16**(5): p. 1366-1378.
53. Sano, M., et al., *Activation and function of cyclin T-Cdk9 (positive transcription elongation factor-b) in cardiac muscle-cell hypertrophy.* Nat Med, 2002. **8**(11): p. 1310-7.

54. Gressel, S., et al., *CDK9-dependent RNA polymerase II pausing controls transcription initiation.* Elife, 2017. **6**.
55. Shao, W. and J. Zeitlinger, *Paused RNA polymerase II inhibits new transcriptional initiation.* Nat Genet, 2017. **49**(7): p. 1045-1051.
56. Devost, D., et al., *Conformational Profiling of the AT1 Angiotensin II Receptor Reflects Biased Agonism, G Protein Coupling, and Cellular Context.* J Biol Chem, 2017. **292**(13): p. 5443-5456.
57. Calderone, A., et al., *Nitric oxide, atrial natriuretic peptide, and cyclic GMP inhibit the growth-promoting effects of norepinephrine in cardiac myocytes and fibroblasts.* J Clin Invest, 1998. **101**(4): p. 812-8.
58. Burger, C. and K.R. Nash, *Small-Scale Recombinant Adeno-Associated Virus Purification.* Methods Mol Biol, 2016. **1382**: p. 95-106.
59. Bolli, P., et al., *Chromatin immunoprecipitation of adult murine cardiomyocytes.* Curr Protoc Cell Biol, 2013. **Chapter 17**: p. Unit17 14.
60. Mbogning, J. and J.C. Tanny, *Chromatin Immunoprecipitation of Histone Modifications in Fission Yeast.* Methods Mol Biol, 2017. **1528**: p. 199-210.

Figure 1.

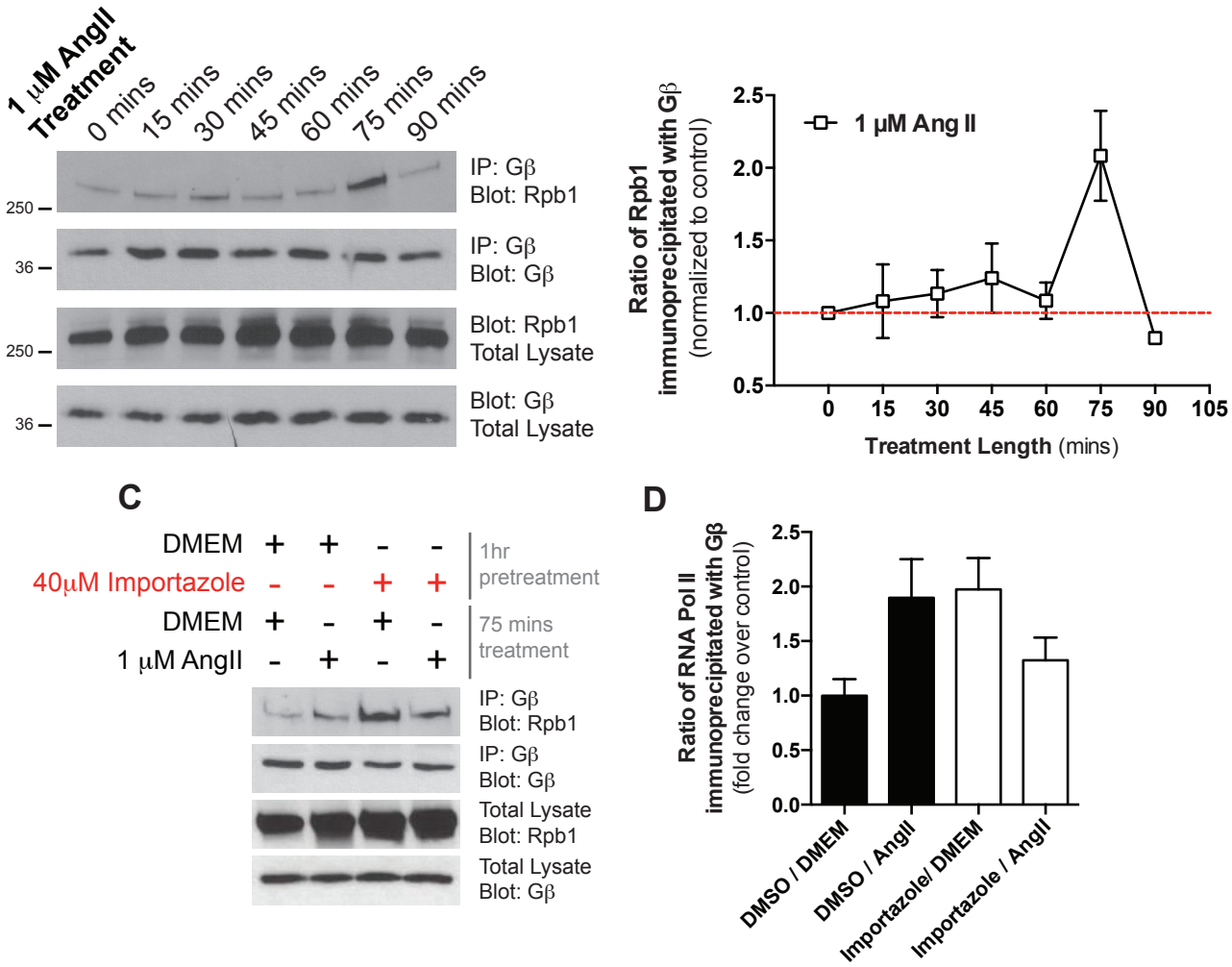

Figure 2.

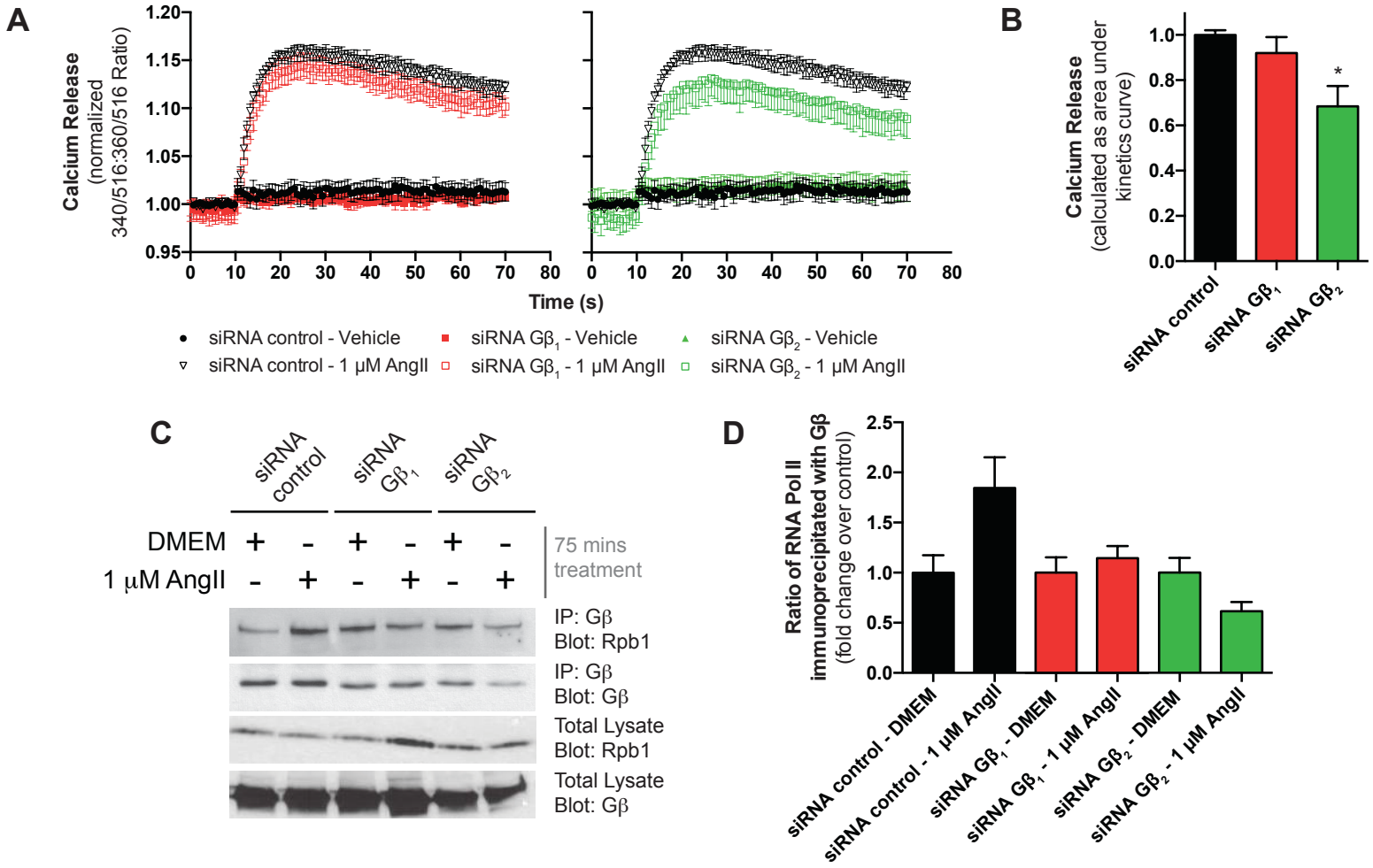

Figure 3.

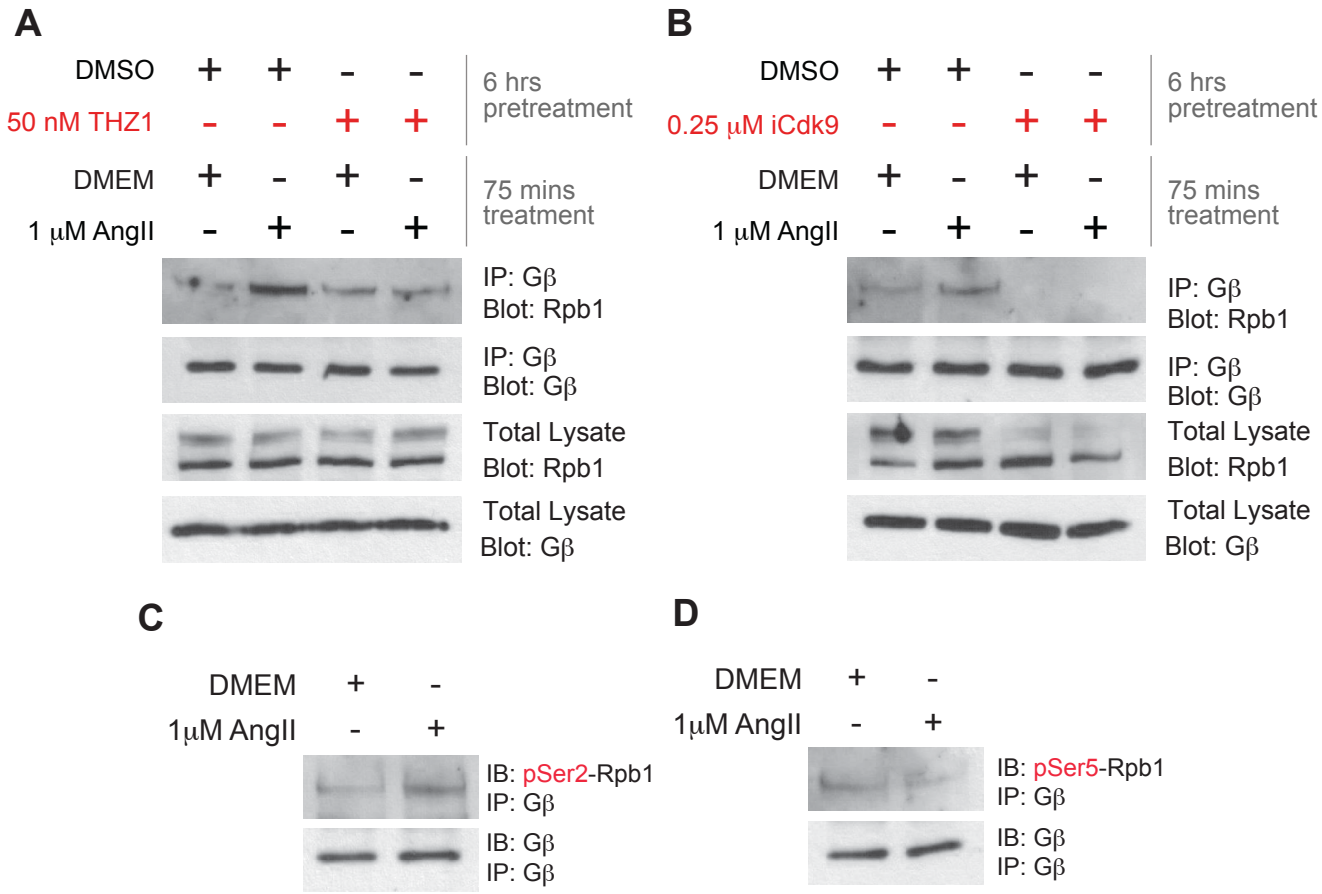

Figure 4.

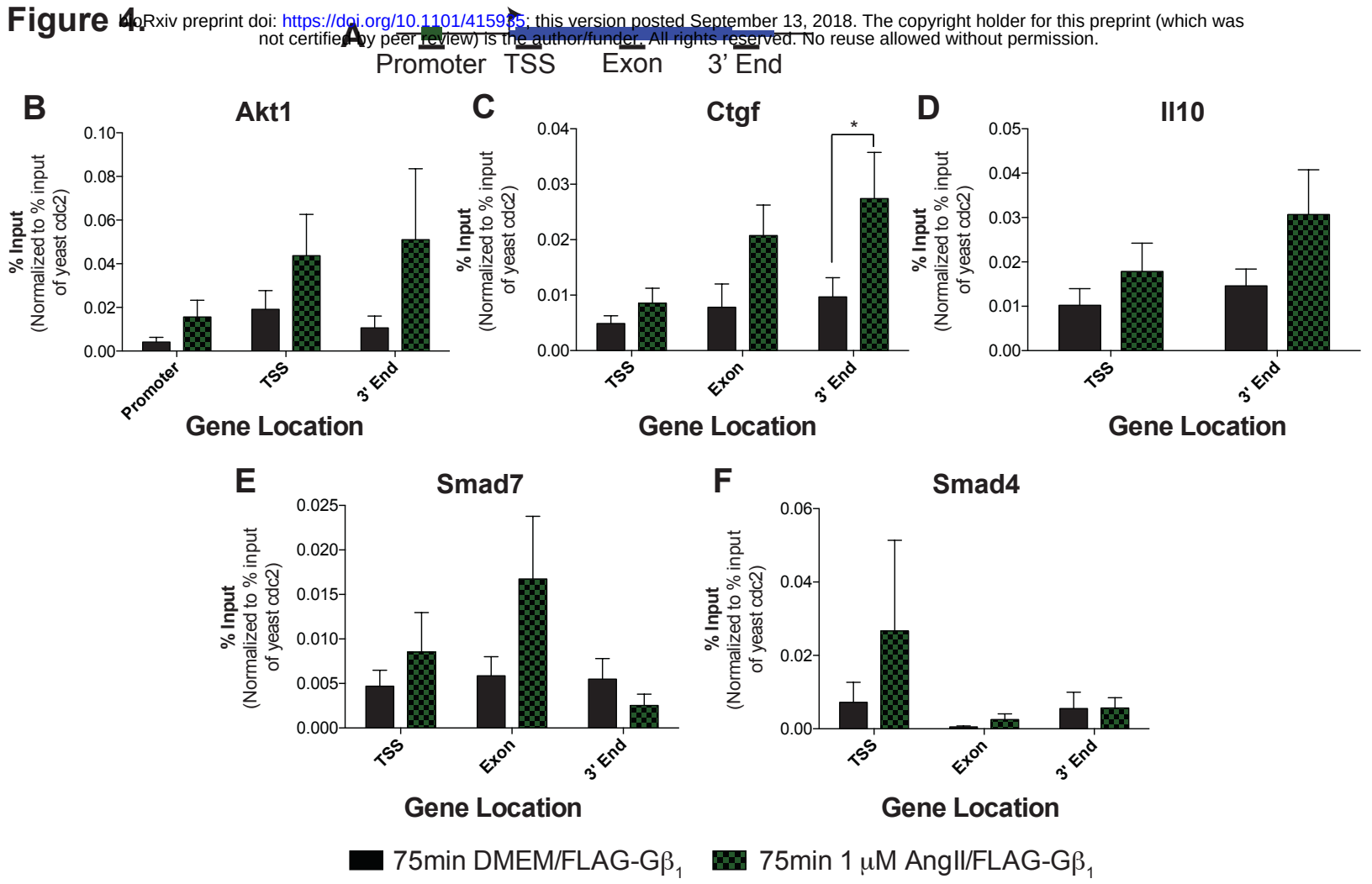

Figure 5.

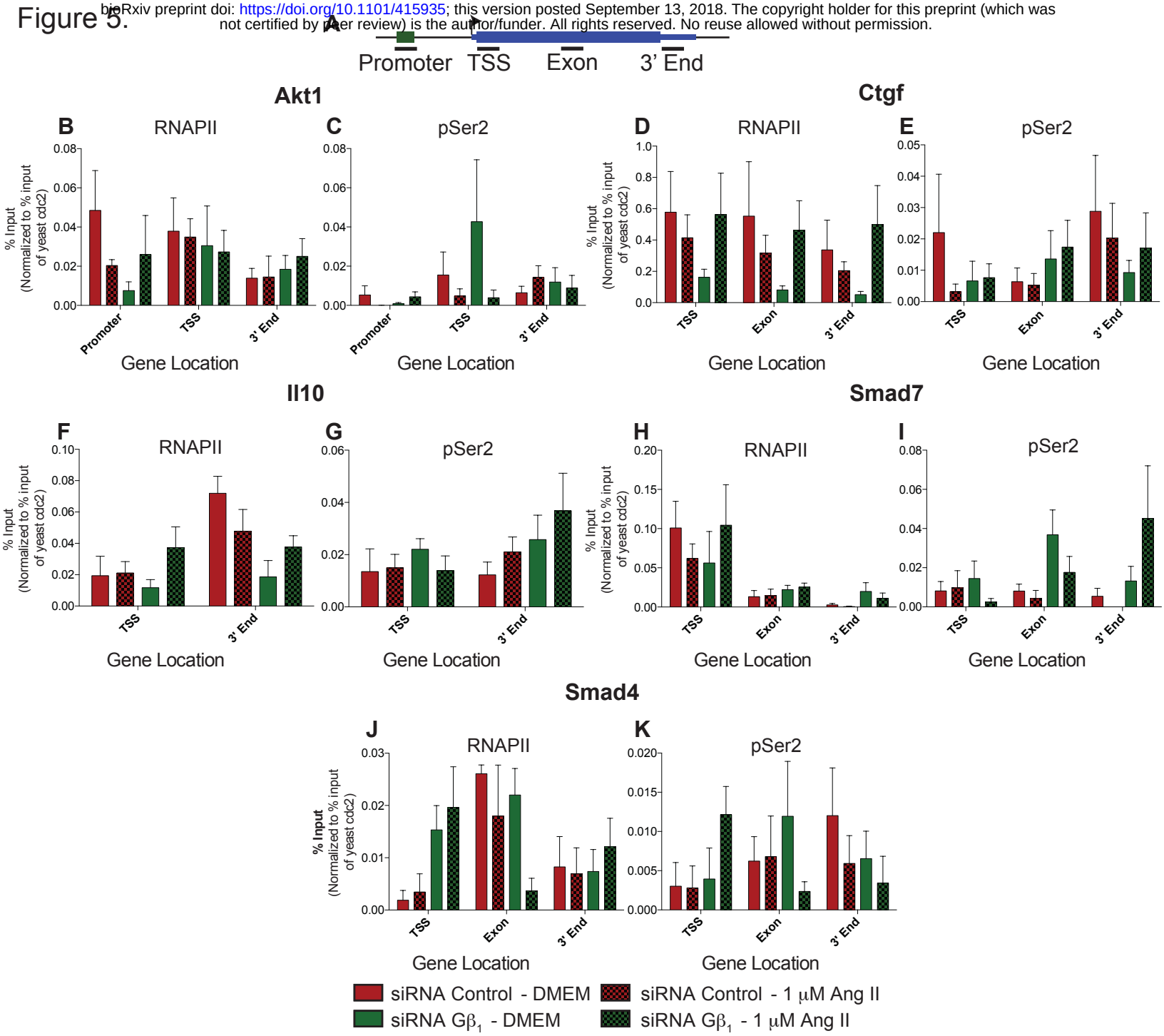

Figure 6.

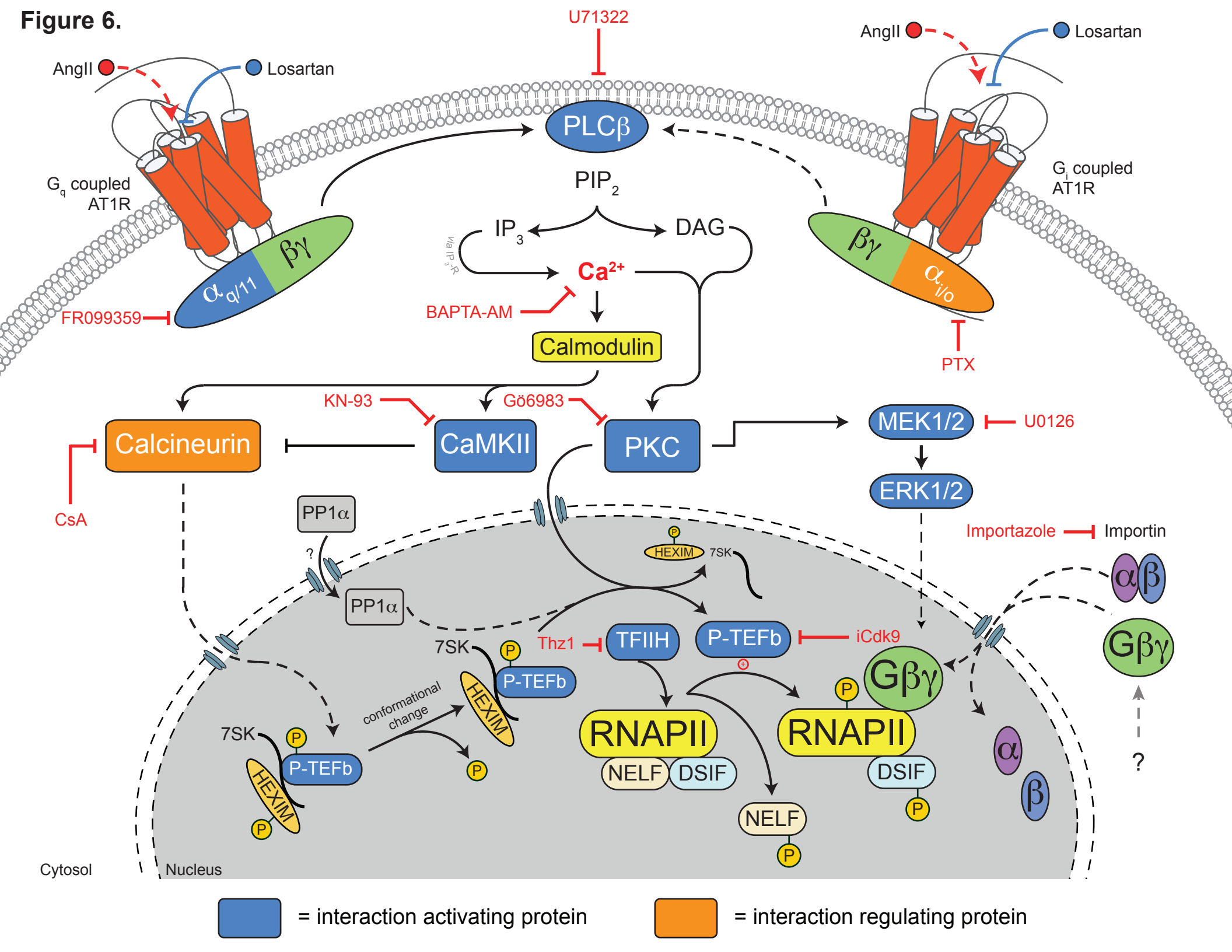
U71322
AngII
Losartan
AngII
Losartan
PLCβ
Gq coupled AT1R
Gi coupled AT1R
PIP2
IP3
DAG
Via IP3R
Ca2+
BAPTA-AM
FR099359
Gαq/11
βγ
βγ
Gαi/o
PTX
Calmodulin
KN-93
Gö6983
Calcineurin
CaMKII
PKC
MEK1/2
U0126
ERK1/2
CsA
PP1α
?
PP1α
HEXIM
7SK
Importazole
Importin
Thz1
TFIIH
P-TEFb
iCdk9
7SK
P-TEFb
HEXIM
conformational change
7SK
P-TEFb
HEXIM
RNAPII
NELF
DSIF
RNAPII
DSIF
NELF
Gβγ
Gβγ
α
β
α
β
?
Cytosol
Nucleus
= interaction activating protein
= interaction regulating protein